Adhesion rupture in laminated glass: influence of adhesion on the energy dissipation mechanisms

Paul Fourton, Keyvan Piroird, Matteo Ciccotti, Etienne Barthel

Challenging Glass 7
Conference on Architectural and Structural Applications of Glass
Ghent University, June 2020.

Adhesion Rupture in Laminated Glass: Influence of Interfacial Adhesion on the Energy Dissipation Mechanisms

Paul Fourton[a], Keyvan Piroird[a], Matteo Ciccotti[b], Etienne Barthel[b]
[a] *Saint-Gobain Research Paris, France, e-mail (keyvan.piroird@saint-gobain.com)*
[b] *SIMM Laboratory, ESPCI, Paris, France*

When laminated glass shatters under impact, most of the energy dissipation occurs in the coupled delamination and stretching of the polymer interlayer between broken chunks of glass. The strong dependency of these mechanisms on interlayer nature, on loading rate and on temperature has been previously investigated: however, the effect of the interfacial adhesion is unexplored. In this work, a surface modification technique is proposed, along with a mechanical characterization of the debonding with the Through Crack Tensile Test. We show that while increasing adhesion has the effect of enhancing the energy required to propagate the delamination fronts as well as the stretch level of the delaminated interlayer, the dissipation associated to the stretching of the volume of the PVB interlayer seems unaffected. We attribute this effect to the competition between the changes in both stretch and stretch rate in the viscoelastic interlayer. Finally, we discuss the experimental observation of the limits of the steady-state debonding regime, related to the competition between adhesive crack propagation and cohesive failure in the interlayer.

Keywords: Laminated Glass, PVB, Adhesion, Through Crack Tensile Test

1. Introduction

The present work focuses on the debonding of a soft polymer material from a glass substrate upon large deformation of the polymer. This subject is related to the impact resistance of laminated glass, an industrial product made of a polymer foil—the interlayer—sandwiched between two glass plies. Previous work on impact resistance of laminated glass showed that for an impacting object of a few kilograms falling on a laminated glass at velocity typically between 1 and 10 m/s, the majority of the kinetic energy is converted into delamination and stretching of the interlayer (Nourry 2005; Elzière et al. 2017).

The key role of the interlayer appears even more clearly in the experimental results of Novotny & Poot (2016). They investigated the effect of temperature on impact performance for 5 different interlayers with the mean break height (MBH) method, a quantitative variation around the "ball drop" test. The MBH procedure consists in dropping a 2-kg steel ball on 30cm×30cm glass panes from a variable height. The drop height is increased when the laminate retains the steel ball ("OK" case), and decreased when the impactor perforates through the glass ("NOK" case). After a few trials, the test sequence oscillated between "OK" and "NOK" cases around the so-called mean break height. These results quantify the strong dependence of impact performance upon the nature of the polymer. In fact, a performance optimum was observed for a temperature correlated to the glass transition temperature.

From the industrial point of view, unveiling the fundamental mechanisms for impact performance would allow better product quality assessment, and also help to create and develop new products. In order to cope with climate change and increased stress on resources, the design of more sustainable building products seems necessary. Innovation goes along with the basic understanding of the physical or chemical processes involved: if we grasp and characterize what phenomena drive impact resistance, then the transition to safer, lighter, and greener products should be facilitated.

The aim of the present work is to investigate the coupling between adhesion, delamination and energy dissipation in a polymer material sandwiched between two glass plies. With the Through-Crack Tensile Test (TCTT) as the principal experimental method, the objective of this work is to have a better understanding of the role of interfacial adhesion in the total energy dissipation in the TCTT system. For that, we modified the glass/PVB interfacial adhesion and studied how this controlled change in interfacial adhesion affects the phenomenology of the TCTT. Notably, we study how the force, stretch and energy are changed during the steady-state delamination. By changing the PVB thickness, we are also able to study the split between dissipation at the debonding front and bulk dissipation in the leg of delaminated PVB.

First, we present the Through Crack Tensile Test (TCTT), how it is relevant to the problem of impact resistance, and a few noticeable results from the literature obtained with this test. In particular, the effects of temperature and loading rate on energy dissipation during steady-state delamination of laminated glass have been thoroughly studied in recent years.

However, the effect of adhesion itself on the phenomenolgy of the TCTT has not received as much attention due to the difficulty in engineering robust and homogenous modifications of interface adhesion. A classical way to change the adhesion is to modify the PVB with additives. We did not choose this way for two reasons: firstly, it is difficult to have a precise and reproducible control of the adhesion in that way. Secondly, by changing the composition of the PVB, we might also unintentionally change the bulk mechanical properties of the PVB. Therefore, to obtain a finely controlled adhesion modification while making sure to have always the same PVB mechanical properties, we chose to make a surface treatment on the glass. We present here an original glass surface treatment protocol based on sol-gel chemistry, which enables to tune the adhesion between a PVB interlayer and glass with a finer control compared to previously reported work. This change of adhesion is assessed using a peel test.

Then, the effect of a known change in adhesion on the phenomenology of the TCTT is investigated. We explore the dependency of steady-state regime limits on the surface chemistry, and the relation between interfacial adhesion and the macroscopic work of debonding.

2. Main results from the literature on the Through-Crack Tensile test

2.1. A model experiment

In his seminal paper, Huntsberger (1981) described the stress state between laminated-glass shards as constrained biaxial extension (Figure 1a). Such loading has been considered by Galuppi & Royer-Carfagni (2017) to develop an analytical model of the post-breakage effective stiffness of a laminated glass panel.

However, it is not straightforward to implement equi-biaxial tension on laminated glass in an experimental test. The stress state has been simplified to uniaxial extension between two glass fragments, as pictured in Figure 1b. Such tensile test between two glass pieces bridged by a polymer ligament has been reported in the literature as the Through Crack Tensile Test—the TCTT—since the late 1990s (Sha et al. 1997; Bennison et al. 1999; Muralidhar et al. 2000; Seshadri et al. 2002). The loading is applied by pulling one of the laminate pieces with a tensile testing machine. The polymer ligament deforms and—if adhesion allows it—delaminates from the glass.

Since it will be our preferred tool in the following, we review here in details the main results from the literature. In the TCTT, the laminate specimen is usually pre-cracked on both glass plies, with two straight parallel cracks. Recent work by Samieian et al. (2018) investigated a "random crack" version of the TCTT, in an effort to rationalize the resistance of laminated glass to blast loading, which we do not consider here.

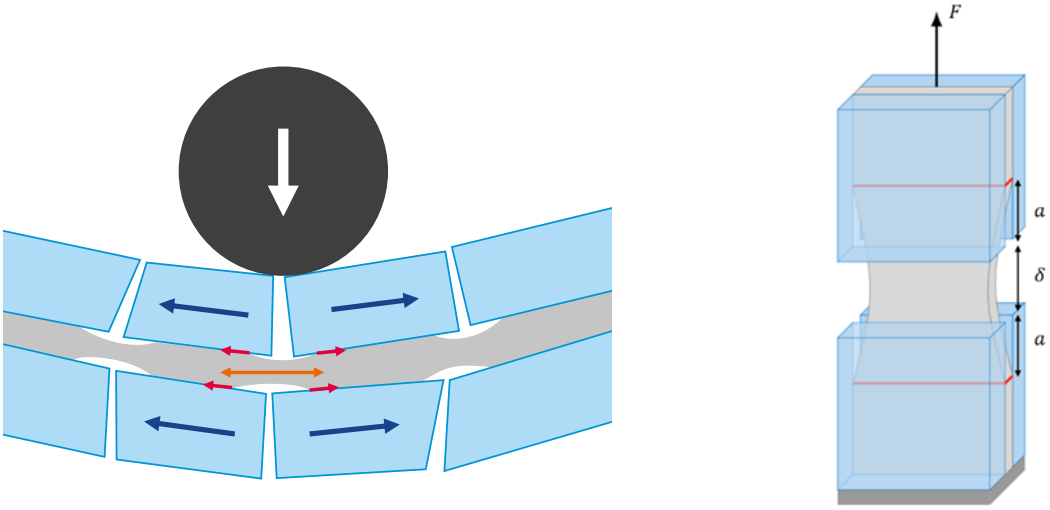

(a) (b)

Figure 1: From the ball-drop test to the TCTT.
(a) Illustration of biaxial tension and delamination between two glass pieces in a ball-drop test, with a laminated glass made of float glass. Arrows merely indicate the relative movement of the glass pieces relative to each other.
(b) Schematic of the Through Crack Tensile Test. In steady-state regime, delamination fronts are essentially straight in the center of the specimen, deviation can occur at the edges.

2.2. Regimes of delamination in the TCTT

In the TCTT, the two laminated glass pieces are originally bridged by the interlayer ligament whose initial length is around tens to a few hundred microns. If delamination does not initiate, the rupture of this interlayer bridge occurs quickly: this is the "rupture regime" observed in high adhesion and high loading rate cases.

Oppositely, in the limit of low adhesion and low loading rates, the polymer debonds in an unstable manner. Unstable debonding means that delamination fronts propagate with irregular profiles, and with an asymmetric behavior. In this regime, crack propagation stops after some initial delamination, which leads to interlayer cohesive rupture.

A remarkable feature of the TCTT is that it presents a steady-state behavior under some intermediate conditions of adhesion, temperature and loading rate. We detail below the characteristics of the steady-state regime, and the energetic analysis it allows.

2.3. The steady-state regime

Steady-state means that, when pulling the two pieces of glass apart at a constant velocity $\dot{\delta}$, we can observe the synchronized propagation of four straight delamination fronts (represented as the red lines in Figure 1b), at an equal and constant velocity $\dot{a}$. This experimental fact has two main consequences:

- The measured force F_{ss} in the steady-state is constant
- The measured average stretch λ_{ss} of the PVB ligament between the fronts also reaches a constant value, after a transitory regime.

Figure 2 shows a typical example of force and stretch measurements during a TCTT in the steady-state regime. The force is measured by the tensile test machine and the stretch is obtained *a posteriori* by image analysis. The delamination fronts positions are tracked as a function of time, so that we measure displacement δ and debonded length $2a$, which allows to determine the average stretch $\lambda = 1 + \delta/2a$. The force reaches a constant value as soon as delamination initiates, while the stretch reaches a plateau after a few seconds.

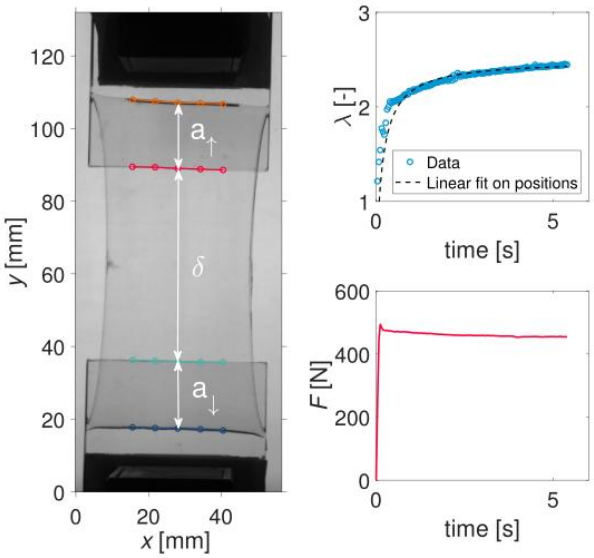

Figure 2: Typical Through Crack Tensile Test with steady state delamination (T = 20°C, $\dot{\delta}$ = 10 mm/s). Clamp displacement is noted δ, delaminated length 2a. Stretch is defined as $\lambda = 1 + \delta/2a$.

The TCTT was at the center of Paul Elzière's PhD thesis (Elzière 2016; Elzière et al. 2017). In the TCTT, it is not straightforward to derive an elastic energy release rate, due to the highly dissipative nature of the polymer materials, which induces a coupling between debonding and large dissipative stretch. However, in the case of steady-state delamination, a well-defined quantity is the total external work injected in the system, which we designate as G_m, the macroscopic work of delamination (analogous to the macroscopic work of fracture from fracture mechanics). The work of delamination is derived from the steady-state force F_{ss}, steady-state stretch λ_{ss}, and the width b_o of the TCTT sample:

$$G_m = \frac{\partial W_{\text{ext}}}{b_0 \, \partial a} = \frac{F_{ss}}{b_o} (\lambda_{ss} - 1) \quad (1)$$

G_m represents the amount of energy injected into the laminated glass per unit of delaminated surface.

The existence of the steady-state regime allows us to study how G_m changes with parameters such as velocity, temperature, interlayer thickness, etc.

2.4. Effect of loading rate

Elzière (2016, 2017) has shown that the steady-state delamination regime is restricted to an intermediate range of tensile velocity, which also depends on the temperature (Figure 3). Recent work by Del Linz et al. (2017) focused on the delamination behavior at high strain rates using a high-speed hydraulic testing machine. In their data, the stretch does not reach a steady value: it increases until rupture of the interlayer, so that we cannot define a consistent $G_m$value. In order to gather data from the literature, we chose to compare the "adherence energy"— i.e. force at the plateau F_{ss} divided by the sample width b_o—in Figure 3.

At low velocities, undulation of the crack fronts leads—though not systematically—to an arrest of the delamination. The stretch increases continuously, until rupture of the interlayer. The empirical "unstable limit" is indicated by the black straight line in Figure 3.

The adherence energy increases with the tensile velocity $\dot{\delta}$: naively, one could think that the higher the velocity, the better the impact performance since more energy can be dissipated. However, the interlayer also bears a higher stress, limited by the strength and toughness of the polymer: the work of delamination is limited by the rupture of the interlayer at high velocities. In the TCTT, the transition from the steady-state regime to the "rupture" regime occurred around 100 mm.s $^{-1}$ at 20 °C, as indicated by the dashed line in Figure 3.

Over the pulling velocity range, from 1 to 10^4 m.s^{-1}, the normalized (debonding) force F_{SS}/b_o increases from 5 to 25 kJ.m $^{-2}$. Such an increase is attributed to viscoelastic dissipation in the PVB interlayer. Indeed, the total debonding energy is expected to increase with $\dot{\delta}$ according to viscoelastic properties of the PVB. The limits drawn from Elzière et al. (2017) are consistent with data from the literature.

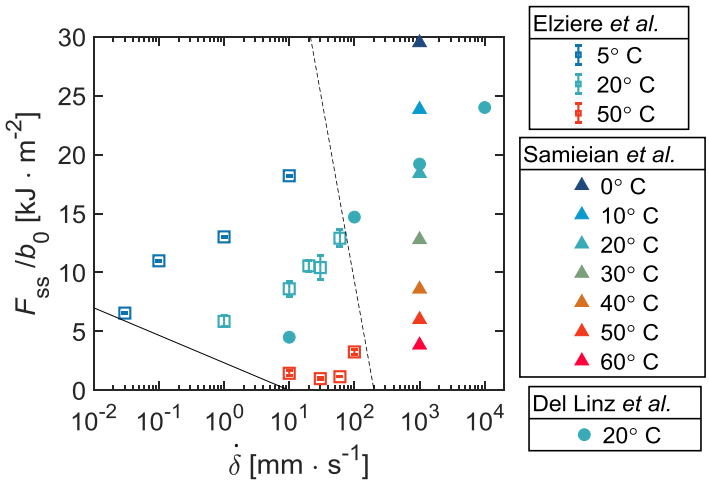

Figure 3: TCTT "phase diagram": normalized force vs. loading displacement rate.
Limits between unstable, steady-state and rupture regimes were drawn by hand to guide the eye.
(Elzière et al. 2017; Samieian et al. 2018; Del Linz et al. 2017)

2.5. Effect of the interlayer thickness

Elzière et al. (2017) also demonstrated that a higher interlayer thickness h_0 increases the delamination force and conversely reduces the average stretch λ_{ss} of the interlayer.

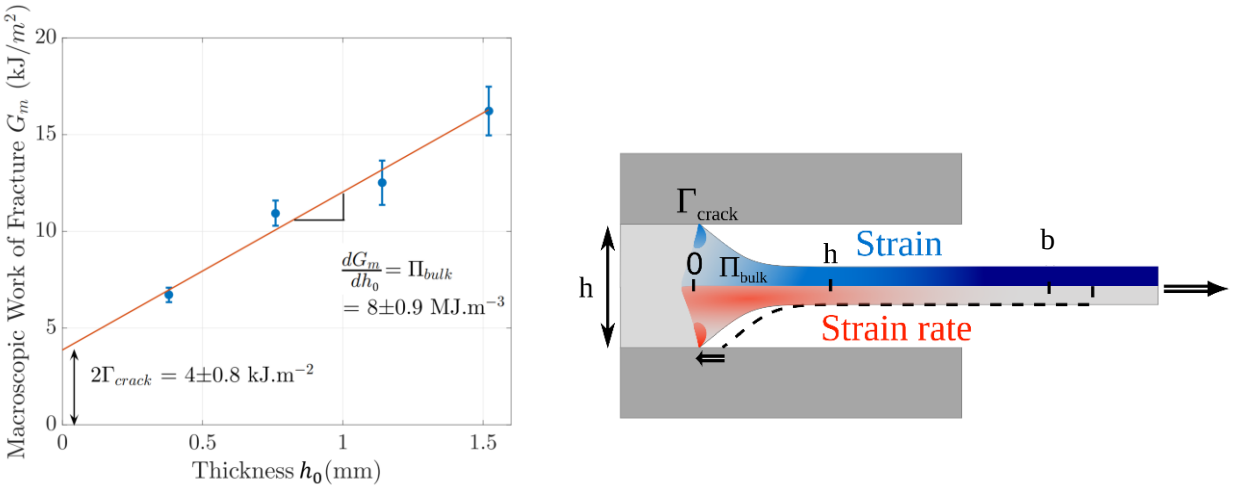

a) (b)

Figure 4: Influence of the thickness on energy dissipation. (a) Macrocopic work of delamination in the TCTT vs. interlayer thickness: affine relationship. (b) Schematic of the energy dissipation regions in the interlayer in the TCTT : (1) at the crack fronts, (2) in a high strain rate zone, (3) in a lower strain rate zone, (4) in a constant stretch zone. From Elzière (2016).

At a given temperature and loading rate, the macroscopic work of delamination G_m increases in an affine manner with the thickness of the interlayer h_0 (Figure 4a). As shown by Elzière et al. (2017), the total work of delamination can be decomposed into a constant term (ordinate at origin) plus a contribution proportional to the thickness h_o:

$$G_m = 2\,\Gamma_{\text{crack}} + h_0\,\Pi_{\text{bulk}} \tag{2}$$

This relation is reminiscent of existing fracture mechanics theories such as the Essential Work of Fracture approach (Bárány et al. 2010). Equation (2) conveys the principle that the effective fracture energy has two distinct contributions: the slope Π_{bulk} is related to (viscoelastic) dissipation in the volume of the stretched interlayer, and the ordinate at origin Γ_{crack} represents the energy required for propagating the crack fronts at the interface. The Γ_{crack} term, of the order of a few kJ/m², involves significant dissipative processes due to strain concentration in the neighborhood the crack fronts (region 1 in Figure 4b).

Butchart & Overend (2012) and Elzière et al. (2017) have characterized the strain field in the interlayer using Digital Image Correlation. Stress concentration at the crack fronts has been evidenced though photoelastic measurements by Ferretti et al. (2012). The main features of the strain and strain rate fields as described in Elzière et al. (2017) are represented in Figure 4b:

- In the vicinity of the crack tip (1), stress concentration occurs. The Γ_{crack} term arises from viscoelastic dissipation in this process zone.
- Zone (2) is the locus of high strain-rates, where most of the bulk viscoelastic dissipation occurs. The interlayer is stretched up to 60%-80% of the macroscopic deformation over a distance close to the thickness h_o, with very limited lateral contraction along the witdh b_0.
- In zone (3), which extends up to a distance about the sample width b_0, the strain rate decreases progressively, and the stretch increases further due to the free lateral contraction along the width b_0.
- In zone (4), the PVB interlayer has reached a constant stretch zone.

Based on this spatial decomposition of the dissipation mechanisms, Elzière et al. (2017) proposed to model the slope Π_{bulk} that relates the macroscopic work of debonding to the thickness h_o, as the work per unit volume required to stretch the interlayer up to its final stretch λ_{ss}:

$$\Pi_{\text{bulk}}(\lambda_{ss}) = \int_1^{\lambda_{\text{ss}}} \sigma^N_{\text{load}}(\lambda)\,\mathrm{d}\lambda \tag{3}$$

Although the stretch proceeds under variable conditions of plane strain in zone (2) and uniaxial strain in zone (3), Elzière et al. (2017) showed that a very good agreement with the experimental data can be obtained by considering for simplicity the estimation of Π_{bulk} through the measurement of the uniaxial extension of the polymer at the high

strain rate of zone (2) where most of the stretch is done. We remark that although the small strain extension of polymers would be quite sensitive to the change of confinement between zones (2) an (3), this effect becomes negligible when considering the energy density associated to the large stretch of incompressible polymers (Treloar 1975).

2.6. Effect of interfacial adhesion

The effect of glass-polymer adhesion on the delamination behavior has been evoked by Sha et al. (1997) using different PVB interlayers. Following the same approach with the TCTT, Franz et al. (2014) have investigated three grades of Trosifol® PVB (BGR10, BG R15, BG R20, Kuraray), ranked from "low" to "medium" to "high" adhesion. However, in their experimental data, "low" and "medium"-adhesion interlayers exhibit the same delamination energy, around 1500 J/m², while the high adhesion interlayer reaches 2500 J/m². Thus, changing the reference of PVB interlayer does not allow a fine and controlled change in adhesion. Moreover, the polymer rheology is not ensured to remain exactly identical when the composition of the interlayer changes.

In the present work, we present a novel approach to this problem: we have modified the glass surface in order to modify in a controlled manner the adhesion between PVB and float glass, while using the same grade of PVB and thus the same bulk rheology.

3. Interfacial adhesion modification by surface treatment on the glass

3.1. Method: sol-gel coating

We used a surface coating made of a mixture of tetraethylorthosilicate (TEOS) and methyltriethoxysilane (MTES) to control the interfacial adhesion between the PVB and the glass. Indeed, PVB adhesion is known to be related to the presence of silanol groups at the surface of the glass, that can form hydrogen bonds with the vinyl alcohol functions of the polymer. The MTES-TEOS system has been reported in the literature—particularly in the 1990s—for coating applications (Innocenzi et al. 1994; Matsuda et al. 1998). Co-condensation of the hydrolyzed silanes was evidenced by ^{29}Si NMR (van Bommel et al. 1991; Fyfe, Aroca 1997; Prabakar, Assink 1997). Co-condensation leads to the formation of a statistical pre-polymer, without phase-separation of the two chemical species. The fine adjustment of the hydroxyl concentration at the glass surface was assumed possible with the MTES-TEOS system. Our main assumption was that a higher TEOS content results in a higher OH density at the surface, which would provide a higher adhesion.

Sols were prepared with a total 1%wt silane concentration in an isopropanol/HCl (pH=1) solvent. The molar ratio between TEOS and MTES is defined as:

$$r_{TEOS} = \frac{n_{TEOS}}{n_{TEOS} + n_{MTES}} \tag{3}$$

We used seven different molar ratio r_{TEOS} between 0 and 1. The silanes were subsequently deposited by wiping technique on the glass.

3.2. Assessment of adhesion modification with the peel test

Peel tests (90° angle) were performed to check the adhesion modification. Samples were conditioned in the testing room at 22°C and 50%RH for 24 hours before the experiment. In order to avoid the stretching of the peeled strand, a stiff fabric backing of thickness *ca.* 0.5 mm is assembled to the polymer. The backing prevents deformation of the polymer layer. A reference value of the peel energy was obtained with PVB adhered onto an untreated float glass substrate. A plateau force F was reached for all samples, and the corresponding adherence energy was calculated as $G_{\text{peel}} = F/b_o$ with $b_o = 20$ mm the width of the PVB strip. As shown in Figure 5, the adherence energy ranged between 0.2 kJ.m^{-2} and 2.5 kJ.m^{-2} and is roughly proportional to r_{TEOS} in the range 10 % - 50 %.

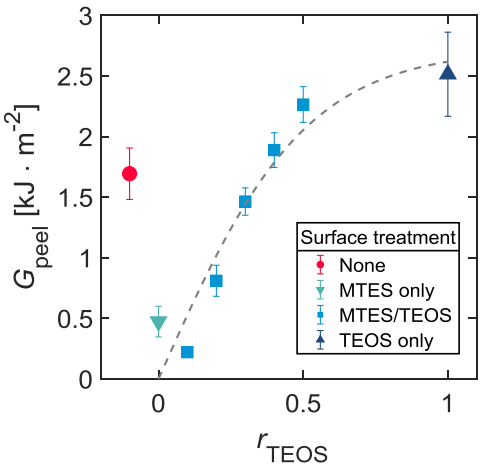

Figure 5: Peel adherence energy vs. TEOS ratio in the surface coating.

3.3. Contact angle measurements

Contact angle measurements (Figure 6) confirmed that the surface was successfully modified: the contact angle was measured around 80° for an advancing water droplet on methylated surfaces. As a reference, the contact angles on clean glass were around 35° (θ_a = 38° , θ_r = 29°). The TEOS-only surface was hydrophilic as the water droplet reached a complete wetting state, to the extent that a reliable contact angle value could not be obtained: the contact angle value was estimated to be less than 5°. Little variation of the contact angle was observed for a TEOS content between 10 and 40 %mol., which was consistent with data from the literature (Matsuda et al. 1998).

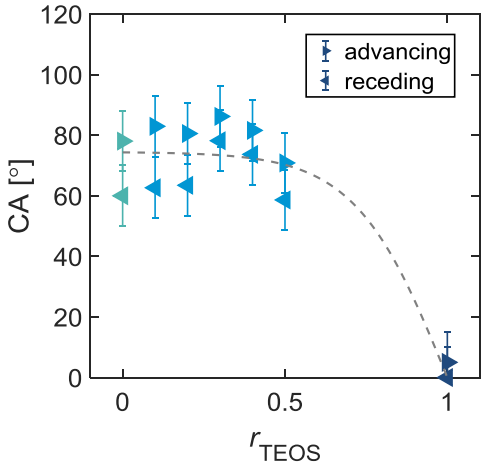

Figure 6: Water contact angle vs. TEOS content in the surface coating.

It is worth noticing that the adherence between PVB and glass did not exhibit a straightforward relationship with the water contact angle. Indeed, adhesion between PVB and glass actually relies on more than polar interaction at the interface. In particular, PVB adheres to glass via hydrogen bonding, and "adhesion modifying" metallic salts also affect the bond strength. Thus, wetting alone cannot predict PVB–glass adhesion, and that is why peel tests are inevitable in order to obtain a meaningful characterization of adhesion.

3.4. Conclusion: peel to estimate Γ_{crack}

Altogether, for our application to mechanical testing, the peel results prove that the adherence between PVB and glass can be controlled and—even better—tuned via the surface chemistry. Although non-standard, our surface modification technique appears to be robust considering the good repeatability of adherence values in the peel test. Furthermore, the adherence appeared to be linear with r_{TEOS} in the range 10%– 50%.

Since the stiff backing prevents the large stretch of the bulk polymer during the peel test, we can suppose that G_{peel} provides a reasonable approximation for the crack propagation energy Γ_{crack} used in the model for the TCTT. Even though G_{peel} is not straightforwardly equal to Γ_{crack} in the TCTT mostly because mode-mixity differs between 90°-peel and TCTT, both values are of the same order of magnitude, *ca.* 1 kJ/m². Indeed, both peel and TCTT "crack"

terms arise from the same intermediate lengthscale where viscoelastic dissipation occurs, between the molecular process zone and the macroscopic scale of the sample dimensions (Creton, Ciccotti 2016). In conclusion we can consider with good approximation that:

$$G_{\text{peel}} \sim \Gamma_{\text{crack}} \propto r_{TEOS} \tag{4}$$

4. Through Crack Tensile Tests with adhesion-modified laminated glasses

Since PVB is hygroscopic, all the necessary precautions to control the moisture content of PVB have been taken. Indeed, Butchart & Overend (2013) have shown with peel tests that a higher moisture content facilitates PVB debonding from the glass. Botz et al. (2019) have investigated the tensile and creep behavior of PVB at various temperatures and humidity ranges, and evidenced that the strong softening of PVB with RH can be modeled by a time-humidity superposition approach for a given temperature.

Prior to sample preparation, the PVB sheet (Saflex® RB41, Eastman) is stored in a cabinet at 23%RH and room temperature (between 20-25°C) for at least 48 hours. After lamination, the samples are again stored in the same cabinet at 23%RH until mechanical testing. The laminate samples are allowed to thermalize at 20°C and ambient humidity in the experimental room with the tensile testing machine for 30 minutes prior to tensile testing. During these 30 minutes, the moisture content is hardly affected: with a diffusion coefficient of water in PVB equal to 3 10^{-6} cm²/min, we find that the moisture only penetrates a few 100 µm from the edges of the sample.

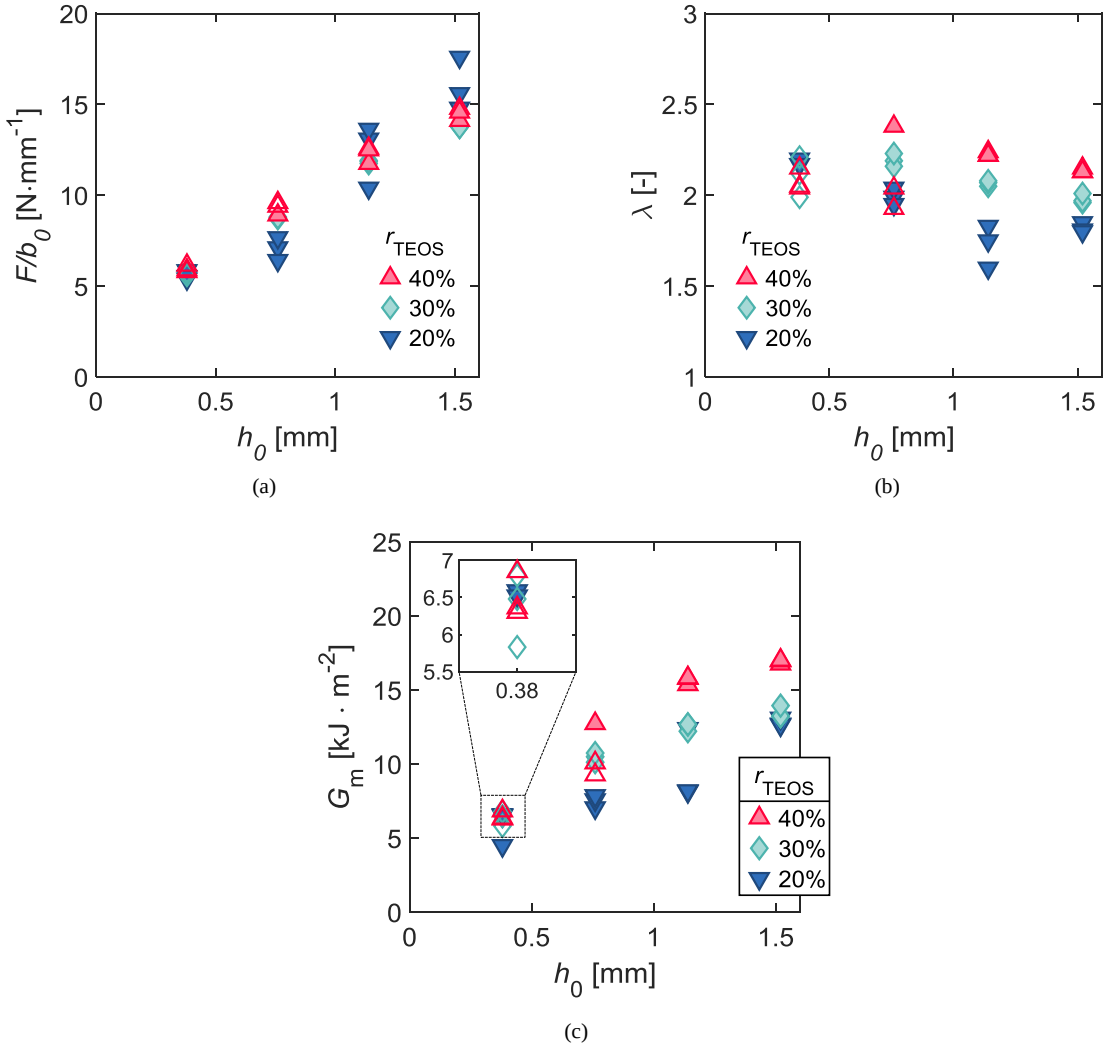

Figure 7: Steady-state TCTT results vs. interlayer thickness: (a) adhesive force, (b) interlayer stretch, (c) macroscopic work of delamination. Filled symbols: steady-state delamination. Hollow symbols: rupture of the interlayer

Through Crack Tensile Tests were performed with glass coated with the MTES-TEOS mix. All the experiments were performed at 20°C and the pulling velocity was set at $\dot{\delta}$=10 mm·s^{-1}. In these conditions we expect a steady-state delamination with standard TCTT samples (2 mm-thick float glass, PVB Solutia® RB41).

The TEOS ratios were 20%, 30% and 40%, which means the adhesive energy varied between *ca.* 1 to 2kJ ·m^{-2}. The goal of this work was to investigate the variation of the "crack" and "bulk" components of the macroscopic work of delamination in the TCTT, according to equation (2), when adhesion between PVB and glass varied with a modified surface chemistry. In these experiments, the PVB thickness was varied between 1 and 4 nominal thicknesses, i.e. between 0.38 and 1.52mm. Three samples were tested for each nominal thickness h_o and each surface treatment.

Figure 7 shows the measured force, the interlayer stretch and macroscopic work of delamination values for each experiment. First, considering only the dependence with the interlayer thickness h_0, our results here are consistent with the literature: at higher interlayer thickness, the force increases while the stretch decreases.

We observed that steady-state was not always obtained, especially for thinner PVB and higher adhesion. In those cases, indicated by hollow symbols in Figure 7, the interlayer ruptured after a partial delamination. In the following, we first analyze the results from steady-state experiments, and secondly the limit cases where interlayer rupture has been observed.

4.1. Analysis of steady-state results

The values of steady-state force were not significantly different for the three coatings (Figure 7a) while the average stretch of the interlayer increased when r_{TEOS} increased (Figure 7b). Consequently, the macroscopic work of delamination increases with r_{TEOS} for a given thickness (Figure 7c). For h_o = 0.76 mm, G_m increases from 7 to 10 to 12kJ·m^{-2} when the TEOS content increased from 20 to 30 to 40% respectively. For a given coating, the trend of G_m vs. h_o appears to be linear considering only the steady-state experiments.

The total macroscopic work of delamination was decomposed into an interfacial "crack" energy and a bulk dissipation contribution according to equation (2) with a linear regression. The ordinate at the origin 2 Γ_{crack} increased with r_{TEOS} (Figure 8a) while the slope Π_{bulk} seemed to be fairly constant (Figure 8b) around the mean value $\overline{\Pi}_{\mathrm{bulk}}$ = 5.2 MJ ·m^{-3} .

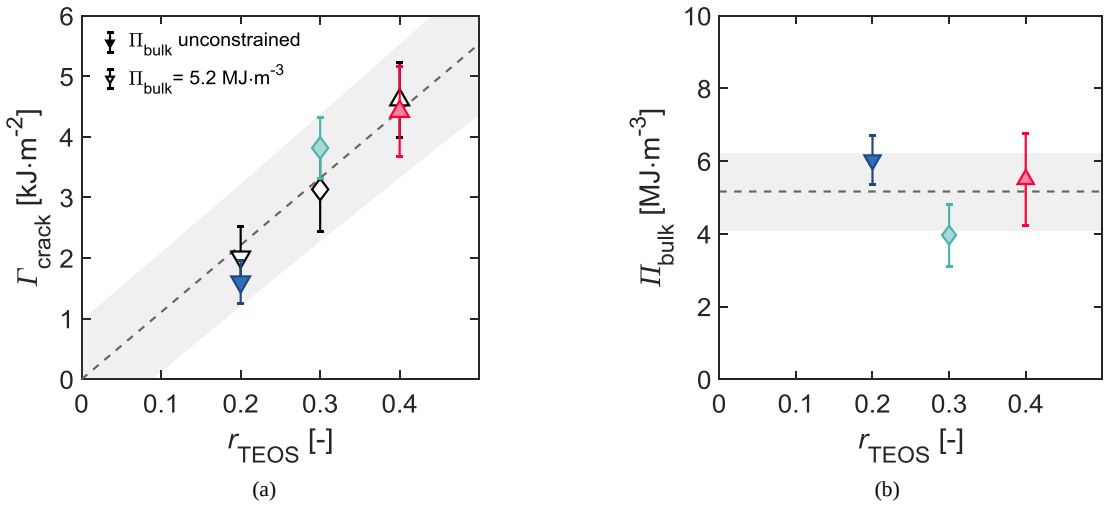

Figure 8: Decomposition of the macroscopic work of delamination.
(a) Crack term vs. TEOS content (error bars: 95% c.i. on coefficients; shaded area: 95% prediction interval of the linear fit Γ_{crack} vs r_{TEOS}).
(b) Bulk term vs. TEOS content (error bars: 95% c.i. on coefficients; shaded area: standard deviation on the mean value $\overline{\Pi}_{\mathrm{bulk}}$).

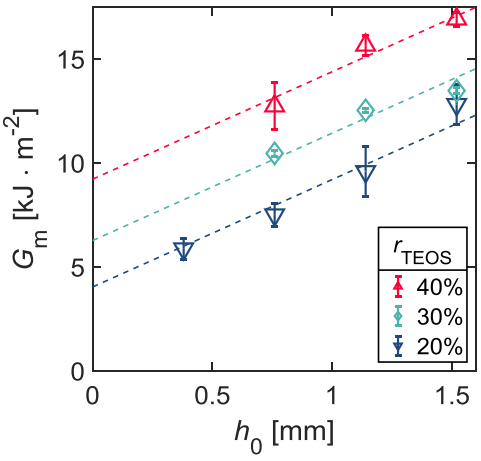

Figure 9: Linear fit of the average macroscopic work of delamination vs. interlayer thickness in the steady-state regime for $\overline{\Pi}_{bulk} = 5.2$ MJ · m^{-3} (error bars: standard deviation, n=3).

The crack contribution from the unconstrained linear regression (filled symbols in Figure 8a) is compared with a linear regression with a fixed value $\overline{\Pi}_{bulk}$ = 5.2 MJ·m−3 (hollow white symbols in Figure 8a). The values of Γ_{crack} are similar between the two fit methods and show a linear trend with respect to the TEOS content in the coating. We have here the experimental confirmation of equation (4), with a factor around 2 between Γ_{crack} in the TCTT and the values obtained in peel (cf. Figure 5).

All in all, the evolution of the work of debonding $G_m(h_0)$ is well described by a linear model with a constant slope, and an ordinate at origin which scales with the TEOS content at the surface (Figure 9). We conclude that the interfacial crack contribution Γ_{crack} scales at the first order with interfacial adhesion, while the bulk contribution Π_{bulk} apparently does not.

4.2. A hand-waving argument for the coupling between adhesion and macroscopic work of delamination

The effect of interfacial adhesion on the crack term follows intuition: a higher adhesion leads to a higher crack propagation energy Γ_{crack}, just like the peel experiments suggest. The increase of the average interlayer stretch required for debonding a tougher interface is also sound. However, the apparent independence of the bulk contribution and of the steady-state force upon interface properties is surprising. We attempt here to rationalize this experimental observation.

For the delamination to propagate, the polymer ligament must carry enough energy to the crack tip, namely an energy Γ_{crack} at each crack front. We suggest an energetic analysis *à la* Rivlin & Thomas (1953) to evaluate this local strain energy release rate G_{crack} in the steady-state regime. Upon adhesive crack propagation, a slice of material is transferred from an unstretched state to a stretched state, characterized by the stretch λ_{ss} and the nominal stress $\sigma_{ss}^N = \sigma_{load}^N(\lambda_{ss})$. The macroscopic work of delamination G_m (work of external forces per unit debonded area) is given by equation (5.a), we express G_m as the product of stress and deformation, after equation (1). In Figure 10, it is represented by the area of the dashed rectangle in the stress-strain curves. Part of this mechanical work is spent into stretching the debonded interlayer: the energy corresponding to stretching is obtained by integrating the loading tensile curve $\sigma_{load}^N(\lambda)$ according to equation (5.b). Note that we use the nominal stress measure (1st Piola Kirchoff stress), since it is the work-conjugate to the stretch. The energy available to propagate the two debonding fronts is the difference between the external work and the energy expended to stretch the debonded interlayer. This corresponds to the complementary energy density of the PVB interlayer (the horizontally striped area in Figure 10b,c). This complementary energy density Π_{comp} multiplied by h_0 must then be equal to 2 Γ_{crack}.

$$G_m = h_0 \cdot \sigma_{ss}^N (\lambda_{ss} - 1) \tag{5.a}$$

$$G_{stretch} = h_0 \cdot \Pi_{bulk}(\lambda_{ss}) = h_0 \int_1^{\lambda_{ss}} \sigma_{load}^N(\lambda)\, d\lambda \tag{5.b}$$

$$2\,G_{\mathrm{crack}} = G_{\mathrm{m}} - G_{\mathrm{stretch}} = h_0 \cdot \left[\sigma_{ss}^{N}\,(\lambda_{ss} - 1) - \int_{1}^{\lambda_{\mathrm{ss}}} \sigma_{\mathrm{load}}^{N}(\lambda)\,\mathrm{d}\lambda\right] = h_0 \cdot \Pi_{\mathrm{comp}} \qquad (5.c)$$

In the TCTT experiments, the velocity $\dot{\delta}$ at which the glass pieces are separated is imposed. In the steady-state, delamination velocity $\dot{a}$ and macroscopic stretch λ are linked by the following formula (coming from the definition of the stretch):

$$\dot{\delta} = 2\,\dot{a}\,(\lambda - 1) \qquad (6)$$

In the TCTT, strain and strain rate are competing: when the strain is increased (for example due to an increase of Γ_{crack}), the delamination velocity $\dot{a}$ is decreased, and so does the strain rate of the debonded interlayer.

Here, we have to recall that plasticized PVB used in our experiments (Saflex® RB41, Eastman) is highly viscoelastic at 20°C. Therefore, the tensile response of PVB is sensitive to the strain rate: PVB becomes stiffer and more plastic-like when the strain rate increases (Figure 10a). Recently, Elzière et al. (2019) have described the rheological properties of plasticized PVB with a non-linear viscoelasticity model, which accounts for both the pronounced hysteresis and the plastic-like behavior at high strain-rate.

We can then relate adhesion variation to the mechanical behavior of PVB. When adhesion and thus Γ_{crack} is increased, the propagation equation $G_{\mathrm{crack}} = \Gamma_{\mathrm{crack}}$ requires an increase of the complementary energy Π_{comp} and thus of the interlayer stretch λ_{ss} as experimentally observed. In turn this implies a reduction of both the delamination velocity $\dot{a}$ and the strain rate of the debonded interlayer, which softens the mechanical response of PVB as indicated in Figure 10. The compensating effects of increased delamination strain and softened response, allows to qualitatively understand that both the nominal stress (and thus the force) and the bulk energy Π_{bulk} tend to remain constant even if the adhesion is increased.

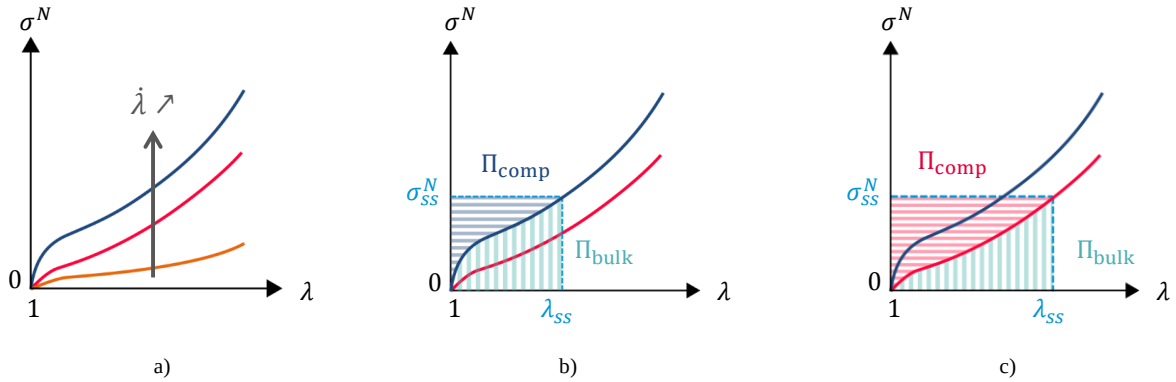

a) b) c)

Figure 10: Schematic of the mechanical response of PVB. (a) Nominal stress vs. nominal strain uniaxial loading curve at increasing strain-rate. (b) Steady-state energy balance at low adhesion. (c) Steady-state energy balance at high adhesion. The area with vertical stripes represents Π_{bulk}, defined in equation 5b and the area with horizontal stripes represents Π_{comp}, defined in equation 5c. Due to the nonlinear material behavior, Π_{bulk} can remain constant while Π_{comp} increases with adhesion.

Clearly, the complexity of the problem calls for a more precise and quantitative analysis, but this hand-waving argument gives the main physical ingredients to take into account.

4.3. Analysis of interlayer rupture limit

The limit between steady-state delamination and interlayer "rupture" behavior was reached with the highest adhesion (r_{TEOS} = 40%) for the two smaller thicknesses. In fact, only one out of three samples at h_o= 0.76 mm exhibited a steady-state behavior, while the two others ended up with a crack initiating from the edges and propagating through the interlayer during the test.

Figure 11 presents an example of rupture behavior for the thinnest PVB. The interlayer remained attached to the left edge of the sample, preventing the delamination there, whereas the crack fronts were straight and horizontal in the central part of the laminate. The stretch increased to λ = 2.3 before a lateral crack started from the left edge and propagated through the interlayer. Consequently, the force decreased when this lateral crack propagated until complete tearing of the interlayer.

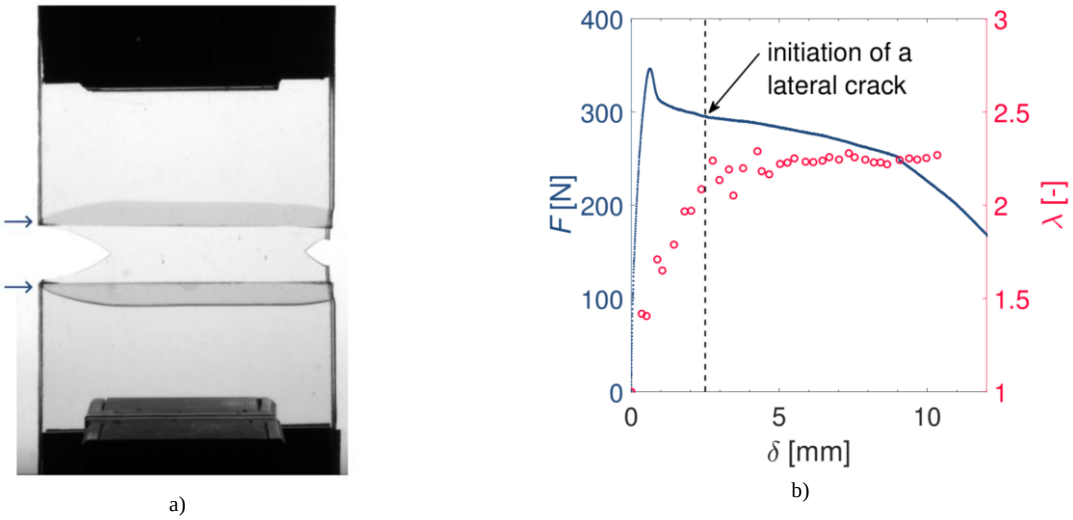

a) b)

Figure 11: Rupture of the interlayer in the TCTT. (a) Snapshot of a TCTT sample during interlayer rupture. Arrows indicate the location where the delamination fronts are blocked. (b) Force and stretch vs. displacement.

Consequently, the values of stretch for those ruptured samples – hollow symbols in Figure 7– were lower than the steady-state value λ_{ss}= 2.4. At the smallest thickness h_o= 0.38mm, for both intermediate (r_{TEOS} = 30%) and high adhesion (r_{TEOS} = 40%) the TCTT resulted in the rupture of the interlayer after a partial delamination. For the thinner interlayer (h_o= 0.38 mm), rupture occurred for all three samples at r_{TEOS} = 30% and 40%. Looking back at Figure 7, it appears that G_m is bounded around 7 kJ.m-3 for h_o = 0.38 mm.

In practice, a crack is more likely to initiate and propagate into the PVB interlayer at lower thicknesses. Indeed, the true stress (force divided by current cross section) increases from 20 MPa to 35 MPa when h_o diminishes (Figure 12): thinner interlayers bear higher stresses compared to thicker ones.

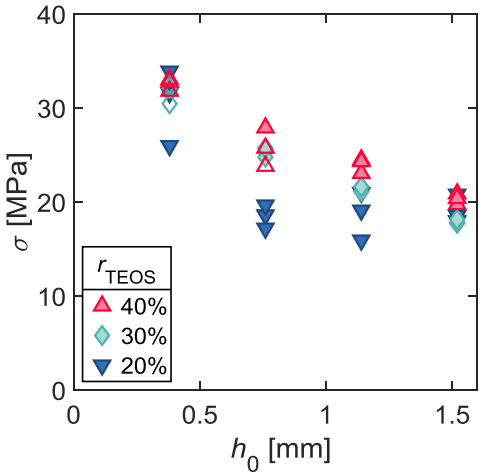

Figure 12: True stress vs. interlayer thickness in the TCTT, for 3 TEOS/MTES surface coatings.

We attribute this limit to the competition between adhesive debonding and cohesive rupture within the interlayer, characterized by the toughness of the polymer material. As stated earlier, the interface debonding propagation criterion is:

$$2\,G_{crack} = h_0 \cdot \Pi_{comp}(\lambda_{ss}) = 2\,\Gamma_{crack} \tag{7}$$

Crack initiation in the PVB interlayer is determined by an intensive criterion, such as a critical stress σ_c *à la Griffith* (1921). When h_0 decreases, the complementary energy must increase to satisfy the crack propagation criterion, which means that both stretch and stress have to increase. Crack initiation occurs when σ_{ss} reaches σ_c. The prediction of this limit would require a thorough study of the rupture envelopes of PVB, and their dependence on loading rate. In practical applications, crack initiation also depends on the size of the largest defect, which makes the analysis even more complex.

5. Conclusion

A methodology based on silane sol-gel chemistry was developed to modify the adherence between PVB and glass. The mix of MTES and TEOS, deposited by a wiping technique, allowed the control of PVB adherence to glass, via the control of the amount of hydroxyl groups exposed at the surface, as quantified by peel tests.

The effect of adhesion on the delamination behavior was assessed with the TCTT with three MTES–TEOS coatings. Destabilization of the crack fronts was observed for lower adhesion and higher PVB thickness, whereas rupture of the interlayer occurred at higher adhesion and lower thickness. Still, a common steady-state regime was observed for all adhesion levels for a PVB thickness of 1.1mm.

In steady-state TCTT, the force surprisingly did not evolve much, while the stretch increased at higher adherence, resulting in a higher work of delamination. The linear evolution of G_{m} with interlayer thickness was decomposed into "crack" and "bulk" dissipation terms: the interfacial crack term intuitively increased when interfacial adhesion increased upon surface modification. However, the volume dissipation term was surprisingly not affected by the adhesion modification. This apparent independence of bulk dissipation upon interface adhesion has been attributed to the compensation of strain rate and stretch effects. At imposed loading rate, lower adhesion implies smaller stretch and thus faster crack propagation and in turn higher strain rate in the debonding region: the effect of smaller stretch and faster strain rate have opposite effects on the volume dissipation term which tend to compensate due to the non-linearity and the rate-dependency of the mechanical response of PVB.

The coupling between viscoelastic rheology and delamination behavior presented here is applicable to plasticized PVB around its glass transition temperature, usually around 20°C. In particular, D. Delincé has investigated the post-breakage response of SentryGlas-laminated glass (Delincé et al. 2008; Delincé et al. 2012; Delincé 2014), for which the mechanical response is much more rigid and plastic, compared to soft and viscoelastic PVB. With this ionomer interlayer, one has to establish a link between deformation, plastic flow, energy dissipation and interfacial debonding. Clearly, some challenges remain in developing a general description of the coupling between material behavior and delamination in laminated glass.

6. References

Bárány, T., Czigány, T., Karger-Kocsis, J.: Application of the essential work of fracture (EWF) concept for polymers, related blends and composites: A review. Prog Polym Sci **35**(10), 1257-1287 (2010). doi:10.1016/j.progpolymsci.2010.07.001

Bennison, S.J., Jagota, A., Smith, C.A.: Fracture of Glass/Poly(vinyl butyral) (Butacite®) Laminates in Biaxial Flexure. Journal of the American Ceramic Society **82**(7), 1761-1770 (1999). doi:10.1111/j.1151-2916.1999.tb01997.x

Botz, M., Wilhelm, K., Siebert, G.: Experimental investigations on the creep behaviour of PVB under different temperatures and humidity conditions. Glass Structures & Engineering **4**(3), 389-402 (2019). doi:10.1007/s40940-019-00098-2

Butchart, C., Overend, M.: Delamination in fractured laminated glass. Proceedings of Engineered Transparency International Conference at Glasstec, Düsseldorf, Germany, 249-257 (2012)

Butchart, C., Overend, M.: Influence of Moisture on the Post-fracture Performance of Laminated Glass. Proceedings of Glass Performance Days 2013, 59-61 (2013)

Creton, C., Ciccotti, M.: Fracture and adhesion of soft materials: a review. Reports on Progress in Physics **79**(4), 046601 (2016)

Del Linz, P., Hooper, P.A., Arora, H., Wang, Y., Smith, D., Blackman, B.R.K., Dear, J.P.: Delamination properties of laminated glass windows subject to blast loading. International Journal of Impact Engineering **105**, 39-53 (2017). doi:10.1016/j.ijimpeng.2016.05.015

Delincé, D.: Experimental approaches for assessing time and temperature dependent performances of fractured laminated safety glass. dissertation, Ghent University (2014)

Delincé, D., Callewaert, D., Vanlaere, W., Belis, J., Depauw, J.: Plastic Deformation of Polymer Interlayers during Post-Breakage Behavior of Laminated Glass - Partim 2: Experimental Validation. International Journal of Modern Physics B **22**(31n32), 5447-5452 (2012). doi:10.1142/s0217979208050632

Delincé, D., Sonck, D., Belis, J., Callewaert, D., Van Impe, R.: Experimental investigation of the local bridging behaviour of the interlayer in broken laminated glass. In: International Symposium on the Application of Architectural Glass ISAAG 2008 Conference Proceedings, Munich, Germany 2008, pp. 41-49

Elzière, P.: Verre feuilleté : rupture dynamique d'adhésion. Ph.D. thesis, Université Pierre et Marie Curie (Paris VI) (2016)

Elzière, P., Dalle-Ferrier, C., Creton, C., Barthel, E., Ciccotti, M.: Large strain viscoelastic dissipation during interfacial rupture in laminated glass. Soft Matter **13**(8), 1624-1633 (2017). doi:10.1039/c6sm02785g

Elzière, P., Fourton, P., Demassieux, Q., Chennevière, A., Dalle-Ferrier, C., Creton, C., Ciccotti, M., Barthel, E.: Supramolecular Structure for Large Strain Dissipation and Outstanding Impact Resistance in Polyvinylbutyral. Macromolecules **52**(20), 7821-7830 (2019). doi:10.1021/acs.macromol.9b01277

Ferretti, D., Rossi, M., Royer-Carfagni, G.: Through-Cracked Tensile Delamination Tests with Photoelastic Measurements. In: Challenging Glass 3, 2012 2012. IOS Press, Delft TU

Franz, J., Schneider, J., Kuntsche, J., Hilcken, J.: Untersuchungen zum Resttragverhalten von Verbundglas: Through-Cracked-Tensile Test. Stahlbau **83**(S1), 241-252 (2014). doi:10.1002/stab.201490063

Fyfe, C.A., Aroca, P.P.: A Kinetic Analysis of the Initial Stages of the Sol−Gel Reactions of Methyltriethoxysilane (MTES) and a Mixed MTES/Tetraethoxysilane System by High-Resolution ^{29} Si NMR Spectroscopy. The Journal of Physical Chemistry B **101**(46), 9504-9509 (1997). doi:10.1021/jp971559x

Galuppi, L., Royer-Carfagni, G.: A homogenized analysis à la Hashin for cracked laminates under equi-biaxial stress. Applications to laminated glass. Composites Part B: Engineering **111**, 332-347 (2017). doi:10.1016/j.compositesb.2016.11.027

Griffith, A.A.: The phenomena of rupture and flow in solids. Philosophical Transactions of the Royal Society of London. Series A, Containing Papers of a Mathematical or Physical Character **221**(582-593), 163-198 (1921). doi:10.1098/rsta.1921.0006

Huntsberger, J.R.: Adhesion of Plasticized Polyvinyl Butyral) to Glass. The Journal of Adhesion **13**(2), 107-129 (1981). doi:10.1080/00218468108073180

Innocenzi, P., Abdirashid, M.O., Guglielmi, M.: Structure and properties of sol-gel coatings from methyltriethoxysilane and tetraethoxysilane. Journal of Sol-Gel Science and Technology **3**(1), 47-55 (1994). doi:10.1007/BF00490148

Matsuda, A., Matsuno, Y., Tatsumisago, M., Minami, T.: Fine Patterning and Characterization of Gel Films Derived from Methyltriethoxysilane and Tetraethoxysilane. Journal of the American Ceramic Society **81**(11), 2849-2852 (1998). doi:10.1111/j.1151-2916.1998.tb02705.x

Muralidhar, S., Jagota, A., Bennison, S.J., Saigal, S.: Mechanical behaviour in tension of cracked glass bridged by an elastomeric ligament. Acta Materialia **48**(18-19), 4577-4588 (2000). doi:10.1016/S1359-6454(00)00244-5

Nourry, E.: Comportement des vitrages feuilletés sous impacts perforants. Ph.D. thesis, ENSAM, Paris (2005)

Novotny, M., Poot, B.: Influence of Temperature on Laminated Glass Performances Assembled with Various Interlayers. Challenging Glass Conference Proceedings **5**, 219-232 (2016). doi:10.7480/cgc.5.2248

Prabakar, S., Assink, R.A.: Hydrolysis and condensation kinetics of two component organically modified silica sols. Journal of Non-Crystalline Solids **211**(1-2), 39-48 (1997). doi:10.1016/S0022-3093(96)00634-5

Rivlin, R.S., Thomas, A.G.: Rupture of rubber. I. Characteristic energy for tearing. Journal of Polymer Science Part A: Polymer Chemistry **10**(3), 291–318 (1953). doi:https://doi.org/10.1002/pol.1953.120100303

Samieian, M.A., Cormie, D., Smith, D., Wholey, W., Blackman, B.R.K., Dear, J.P., Hooper, P.A.: Temperature effects on laminated glass at high rate. International Journal of Impact Engineering **111**, 177-186 (2018). doi:10.1016/j.ijimpeng.2017.09.001

Seshadri, M., Bennison, S.J., Jagota, A., Saigal, S.: Mechanical response of cracked laminated plates. Acta Materialia **50**(18), 4477-4490 (2002). doi:10.1016/S1359-6454(02)00255-0

Sha, Y., Hui, C.Y., Kramer, E.J., Garrett, P.D., Knapczyk, J.W.: Analysis of adhesion and interface debonding in laminated safety glass. Journal of Adhesion Science and Technology **11**(1), 49-63 (1997). doi:10.1163/156856197X01010

Treloar, L.R.G.: The Physics of Rubber Elasticity. Oxford University Press, USA, (1975)

van Bommel, M.J., Bernards, T.N.M., Boonstra, A.H.: The influence of the addition of alkyl-substituted ethoxysilane on the hydrolysis—condensation process of TEOS. Journal of Non-Crystalline Solids **128**(3), 231-242 (1991). doi:10.1016/0022-3093(91)90461-E

7. Conflict of interest

The authors declare they have no conflict of interest.